Analysis of the Strengthening Mechanism Based on Stress-Strain Hysteresis Loop in Short Fiber Reinforced Metal Matrix Composites

Hong Gun Kim* and Ik Chang**

(Received August 3, 1994)

The strengthening mechanism of short fiber or whisker reinforced metal matrix composites has been studied by a continuum mechanics treatment utilizing finite element analysis (FEA). To assess the tensile and compressive constitutive responses, a constraint-unconstraint comparative study based on stress-strain hysteresis loop has been performed. For analysis procedures, the aligned axisymmetric single fiber model and the stress grouping technique have been implemented to evaluate the domain-based field quantities. Results indicate that the development of significant triaxial stresses within the matrix both for the tensile and compressive loading, due to the constraint imposed by reinforcements, provide an significant contribution to strengthening. It was also found that fiber stresses are not only sensitive to the fiber/fiber interaction effects but also substantially contribute to the composite strengthening both for the tensile and compressive loading.

Key Words : Stress-Strain Hysteresis, Metal Matrix Composites, Hydrostatic Stress, Constraint Effect, Triaxiality, Strengthening Mechanism

1. Introduction

Metal matrix composite (MMC) is one of the strongest candidates as a structural material for many high-temperature and aerospace applications (Divecha, Fishman, and Karmarkar, 1981 ; Nair, Tien, and Bates, 1985 ; Kelly and MacMillan, 1986). The main objective of using MMCs is to increase service temperature or specific mechanical properties of structural components by replacing existing superalloys. In these MMCs, mechanisms of strengthening and of microscopic deformation were issues of academic and practical importance. Many different strengthening mechanisms have been proposed, which include : (1) Overall strengthening directly attributable to the strength of individual components of the composite as per the mixture theories (Cho and Gurland, 1988), (2) strengthening due to long-range image stress (or back stress) in the plastically deforming composite matrix and due to plastic relaxation by the formation of prismatic dislocation loops around the hard particles (Mori and Tanaka, 1973), (3) Load transfer between the fiber and the matrix (Nardone and Prewo, 1986 ; Nardone, 1987), (4) Enhanced dislocation density in the matrix (Arsenault and Fisher, 1983 ; Arsenault, 1984 ; Arsenault and Shi, 1986), (5) Residual stresses due to thermal mismatch between the components (Koss and Copley, 1971 ; Arsenault and Taya, 1987), (6) Strengthening arising from constrained plastic flow in the ductile matrix due to the presence of brittle reinforcements (Drucker, 1965 ; Christman, Needleman, and Suresh, 1989 ; Kim, 1992 ; Kim, 1994a ; Kim et al., 1994).

A thorough evaluation of the merits of various

*Department of Mechanical Engineering, Jeonju University, 1200 Hyoja-Dong 3 Ga, Wansan-Gu, Jeonju 560-759, Korea.

**Department of Industrial Engineering, Jeonju Technical College, 72 Namnosong-Dong, Wansan-Gu, Jeonju 560-761, Korea.

arguments for strengthening in MMCs is often difficult because of the paucity of complete information on the processing, characterization, and properties of the materials. The first and second theories provide approximate predictions of composite response. However, Those are restricted to ellipsoidal reinforcement geometry for which case the internal reinforcement stress is assumed to be uniform. It is well known that for the case of rod-like fiber geometries, uniform reinforcement stresses are obtained only at sufficiently large aspect ratios. The uniform internal reinforcement stress results from the physical nature of the ellipsoidal geometry for which case both normal and shear load transfer to the reinforcement occurs along the entire fiber/matrix boundary. For an axially aligned cylindrical geometry, however, with the load applied in the axial direction, the normal stress transfer occurs only at the fiber end and the stress transfer along the fiber length is purely of a shear nature. This shear stress transfer gives rise to the known variation of the fiber axial stresses (Piggot, 1980). This phenomenon is related to the plastic deformation evolution that is important to appreciate the strengthening induced by fiber/fiber interactions.

On the other hand, some theories of composite strengthening have been proposed that directly relate the composite yield strength to the yield strength of the matrix. Enhanced dislocation density in the matrix of the reinforced alloys is related to the observations of a high density of dislocations generated in the composite matrix during cooling from the processing temperatures due to difference in the coefficient of thermal expansion between the fiber and matrix (Arsenault and Shi, 1986 ; Vogelsang, Arsenault, and Fisher, 1986 ; Taya and Mori, 1987 ; Derby and Walker, 1988). The load transfer mechanism between the fiber and matrix (Nardone, 1986 ; Nardone and Prewo, 1987) also relates to the composite yield strength and predicts that the composite strength is linearly related to the matrix yield strength. Here, the composite yield strength is taken to be the 0.2% yield strength. However, since the composite stress-strain curve is typically rather smooth, characterization of the stress-strain response in terms of a yield strength is incomplete. It should also be noted that the yield strength value is sensitive to the precise definition of composite yielding.

Further, it would be expected that the difference in dislocation densities be reflected in an increase in microhardness values for the reinforced matrix material (Arsenault and Fisher, 1983 ; Arsenault, 1984). However, this is not observed experimentally for the 2124 SiC whisker composite system where the range of microhardness values for the composite matrix is roughly the same as that of the control alloy (Christman, Needleman, and Suresh, 1989). Also, in a SiC particulate reinforced Al-4% Cu composite system, the microhardness value of a peak aged matrix was found to decrease with increasing volume fraction of the reinforcement, despite significant increases in the measured yield strength of the composite (Christman, Needleman, and Suresh, 1989).

Residual stresses due to thermal mismatch between the components were proposed as one of the contributors of strengthening mechanism (Koss and Copley, 1971 ; Arsenault and Taya, 1987). However, it has been presented that the residual stress effects do not make a significant difference in the overall constitutive responses (Levy and Papazian, 1991 ; Nair and Kim, 1991). Furthermore, the localized high dislocation densities would result in a work hardened matrix which may be more susceptible to the subsequent deformation and failure (Kim, 1992).

Finally, the strengthening mechanism arising from constrained plastic flow (Drucker, 1965 ; Christman, Needleman, and Suresh, 1989) has been investigated for the composite tensile behavior. In their studies, it was reported that the constrained plastic flow generates the Triaxiality in the matrix so that the role of matrix is significant more than any other factors. However, Kim (1992) suggested that the role of fiber may be the major contributor for composite strengthening through the analysis of tensile stress-strain behavior. It seems important to understand that the results of unconstrained representative volume element (RVE) is not realistic as reported in the

previous study (Nair and Kim, 1991 ; Kim, 1992). Thus far, a comparative study between constrained and unconstrained model must give an insight from where the composite strengthening stems.

In this paper, therefore, an attempt to characterize the major composite strengthening mechanism in MMCs has been given in detail through a constraint-unconstraint comparative study implementing an elastoplastic FEA and stress grouping approach. It was found that this approach provides a rationale through the constitutive characteristics in MMCs (see section 3). An axisymmetric single fiber model based on incremental plasticity theory using von Mises yield criterion and Plandtl-Reuss equations was employed to evaluate both the constrained and unconstrained RVE. A domain-based stress grouping technique was implemented to obtain the stress-strain hysteresis loop that gives the information of tensile and compressive constitutive responses in a designated region. It was found that the contribution of overall matrix is not significant though it generates a source of strengthening. Finally, comparisons with other strengthening theories were discussed in detail.

2. Finite Element Formulations for Elastoplastic Analysis

The FE formulations in this work are centered on the elastoplastic analysis with small strain plasticity theory (Cook, Malkua, and Plesha, 1989) using an axisymmetric single reinforcement model. To solve nonlinearity, Newton-Raphson method has been implemented in this study. Consistent with small strain theory,

$$\{d\varepsilon^{el}\}=\{d\varepsilon\}-\{d\varepsilon^{pl}\} \tag{1}$$

where $\{d\varepsilon\}$, $\{d\varepsilon^{el}\}$and $\{d\varepsilon^{pl}\}$ are changes in total, elastic, and plastic strain vectors, respectively. Elastoplastic stress-strain matrix can be solved iteratively, in which the elastic strain vector is updated at each iteration, and the element tangent matrix is also updated. For a static analysis, the FE discretization process yields a set of simultaneous equations :

$$[K]\{u\}=\{F^a\} \tag{2}$$

where $[K]$ is the stiffness matrix, $\{u\}$ is a set of displacements, and $\{F^a\}$ is a set of applied loads. By Newton-Raphson method, the path dependent non-linearity can be accomplished effectively by using a step by step incremental analysis, i. e., the final load $\{F^a\}$ is reached by stepping the load in increments and performing the Newton-Raphson iterations at each step :

$$[K_{m,n}]\{\Delta u_n\}=\{F_m^a\}-\{F_{m,n}^{nr}\} \tag{3}$$

$$\{u_{n+1}\}=\{u_n\}+\{\Delta u\} \tag{4}$$

where $[K_{m,\ n}]$ is the tangent stiffness matrix for load step m, and iteration n, $\{F^{nr}{}_{m,n}\}$ is the restoring force for load step m and iteration n, and $\{F_m^a\}$ is the total applied force at load step m. At each iteration of a load step, Both $[K_n]$ and $\{F_n^{nr}\}$ are evaluated based on the configuration given by $\{u_n\}$ and the preset criterion for convergence, i. e. plasticity ratio was used as 1% at all integration points in the model. The element tangent matrix $[K_{e,n}]$ and the element Newton-Raphson restoring vector $\{F^{nr}{}_{e,n}\}$ in the nth iteration are :

$$[K_{e,n}]=\int_V [B]^T[D_{ep,n}][B]dV \tag{5}$$

$$\{F_{e,n}^{nr}\}=\int_V [B]^T[D_{ep,n}]\{\varepsilon_n^{el}\}dV \tag{6}$$

where $[B]$ is the strain-displacement matrix, $[D_{ep,n}]$ is the elastoplastic stress-strain matrix. The derivation of $[D_{ep}]$ is as follows. The yield criterion determines the stress level at which yielding is initiated. For an elastoplastic material, a yield function F which is a function of stresses $\{\sigma\}$ and quantities $\{\alpha\}$ and associated with the hardening rule can be defined. Yielding occurs when

$$F(\{\sigma\},\ \{\alpha\},\ \kappa)=0 \tag{7}$$

where K is the plastic work per unit volume and $\{\alpha\}$ is the translation of yield surface. Specifically, the $\{\alpha\}$ is history dependent, i. e.,

$$\{\alpha\}=\int C\{d\varepsilon^{pl}\} \tag{8}$$

$$\kappa=\int\{\sigma\}^T\{d\varepsilon^{pl}\} \tag{9}$$

where C is a material parameter. According to von Mises theory, yielding begins under any states

of stress when the effective stress σ_e exceeds a certain limit, where

$$\sigma_e=\left[\frac{1}{2}\{(\sigma_x-\sigma_y)^2+(\sigma_y-\sigma_z)^2+(\sigma_x-\sigma_z)^2\}+3(\tau_{xy}^2+\tau_{yz}^2+\tau_{xz}^2)\right]^{1/2} \tag{10}$$

The flow rule determines the direction of plastic straining. A plastic potential Q which has a unit of stress and is a function of stresses (that determines the direction of plastic straining), $Q=Q(\{\sigma\}, \{\alpha\}, K)$, a scalar which is called a plastic multiplier (that determines the amount of plastic straining), plastic strain increments are given by

$$\{d\varepsilon^{pl}\}=\lambda\left\{\frac{\partial Q}{\partial\sigma}\right\} \tag{11}$$

where $\{d\varepsilon^{pl}\}$ is the incremental plastic strain. The hardening rule describes the change of the yield surface with progressive yielding, so that the conditions, i. e., the yield surface in stress space. Equation (7) can then be differentiated so that

$$dF=\left\{\frac{\partial F}{\partial\sigma}\right\}^T\{d\sigma\}+\left\{\frac{\partial F}{\partial\alpha}\right\}^T\{d\alpha\}+\frac{\partial F}{\partial x}dx=0 \tag{12}$$

Noting from Eqs. (8) and (9) that

$$\{d\alpha\}=C\{d\varepsilon^{pl}\} \tag{13}$$

$$dx=\{\sigma\}^T\{d\varepsilon^{pl}\} \tag{14}$$

Using Eqs. (13) and (14), Eq. (12) becomes

$$\left\{\frac{\partial F}{\partial\sigma}\right\}^T\{d\sigma\}+\left\{\frac{\partial F}{\partial\alpha}\right\}^T C\{d\varepsilon^{pl}\}+\frac{\partial F}{\partial x}\{\sigma\}^T\{d\varepsilon^{pl}\}=0 \tag{15}$$

The stress increment can be computed via the elastic stress-strain relations as follows:

$$\{d\sigma\}=[D]\{d\varepsilon^{el}\}=[D](\{d\varepsilon\}-\{d\varepsilon^{pl}\}) \tag{16}$$

Substituting Eq. (12) into Eqs. (15) and (16) and combining Eqs. (15) and (16):

$$\lambda=\{C_\lambda\}^T\{d\varepsilon\} \tag{17}$$

where

$$\{C_\lambda\}=\frac{\left\{\frac{\partial F}{\partial\sigma}\right\}^T[D]}{\left\{\frac{\partial F}{\partial\sigma}\right\}^T[D]\{d\sigma\}-C\left\{\frac{\partial F}{\partial\alpha}\right\}^T\left\{\frac{\partial Q}{\partial\sigma}\right\}-\frac{\partial F}{\partial k}\{\sigma\}^T\left\{\frac{\partial Q}{\partial\sigma}\right\}} \tag{18}$$

The size of plastic strain increment is therefore related to the total increment in strain, the current stress state and the specific forms of the yield and potential surfaces. The plastic strain increment is then computed using Eq. (11). The tangent or elastoplastic stress-strain matrix can then be derived by Eq. (16):

$$\{d\sigma\}=[D](\{d\varepsilon\}-\{d\varepsilon^{pl}\}) \tag{19}$$

Using the definition of $\{d\varepsilon^{pl}\}$ and in λ Eqs. (11) and (17):

$$\{d\sigma\}=[D_{ep}]\{d\varepsilon\} \tag{20}$$

where the elastoplastic matrix $[D_{ep}]$ is

$$[D_{ep}]=[D]\left(1-\left\{\frac{\partial Q}{\partial\sigma}\right\}\{C_\lambda\}^T\right) \tag{21}$$

Incorporating associated flow rule (Plandtl-Reuss equation) and isotropic hardening rule, $Q=F$ and $\{\alpha\}=\{0\}$ have been implemented in this study.

3. Model and Materials

3.1 Model

The micromechanical model to describe a short fiber reinforced composite is an axisymmetric single fiber RVE. The FE meshes of quadrant geometry due to symmetry is shown in Fig. 1. In this model, a uniform fiber distribution with an end gap value equal to transverse spacing between fibers was selected as has been done by Agarwal, Liftsiz, and Broutman (1974), Nair and Kim

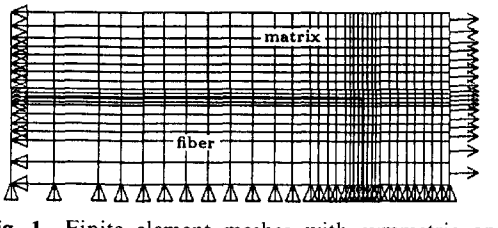

Fig. 1 Finite element meshes with symmetric and loading boundary conditions ($V_f=0.2$).

(1991), and Kim (1994b). The fibers were assumed as uniaxially aligned with no fiber/matrix debonding allowed for, in keeping with the actual situation in many MMCs. For instance, Arsenault (1983), Arsenault and Fisher (1983), and Arsenault and Pande (1984) showed that the bonding strength between SiC and Al and between W and Cu is very good. It strongly supports that the perfect bonding assumption is fairly reasonable for the load transfer between the matrix and the reinforcement. With respect to fiber alignment, Takao, Chou, and Taya (1982) concluded that a misorientation angle of less than 10° has little effect on the composite stiffness, while a misorientation angle greater than 15°~20° has a great effect. Quantitative measurement of the fiber misorientation of this material were not made, but visual observations confirmed that the extrusion process has caused a high degree of fiber alignment. In the previous work (Levy and Papazian, 1991), the longitudinal and transverse predictions of the FE models were compared to experimental measurements of longitudinal properties, and it was concluded that the effects of fiber misorientation were not of first order significance for the samples. The constraint boundary condition enforces elastic and plastic constraint by requiring that the radial and axial boundary of RVE is maintained in the straight manner during deformation.

On the other hand, the concept of volume average method has been implemented to produce the domain-based stress-strain responses. The overall stress in a domain can be calculated through a simple averaging scheme given by the following equation :

$$<\sigma_{ij}>_{\Omega}=\frac{\int_{\Omega}(\sigma_{ij})_k V_k d\Omega}{\int_{\Omega} V_k d\Omega} \tag{22}$$

where $(\sigma_{ij})_k$ is the stress in element k and V_k is the volume of that element. Hence, Eq. (22) is used to group each domain stress. Hence, the average stress-strain response can be obtained in each domain, which represents regional RVE stresses. By employing this stress grouping approach, a representative domain stress-strain curve can be delineated. In a short fiber reinforced composite, the composite domain Ω_c can be decomposed into the fiber region Ω_f and the matrix region Ω_m as shown in Fig. 2. In the same fashion, the field quantity in the matrix region Ω_m

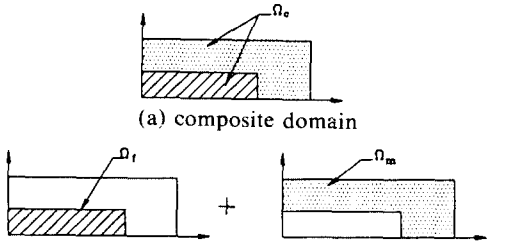

(a) composite domain

(b) decomposed fiber and matrix domains

Fig. 2 A schematic of stress grouping approach in a short fiber or whisker reinforced composite.

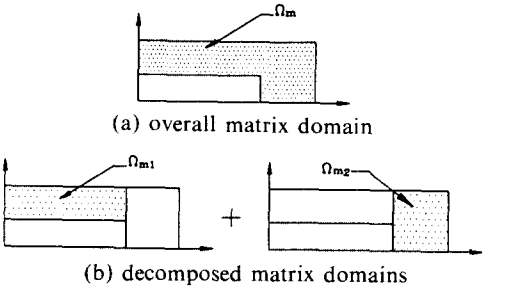

(a) overall matrix domain

(b) decomposed matrix domains

Fig. 3 A schematic of stress grouping approach in the matrix.

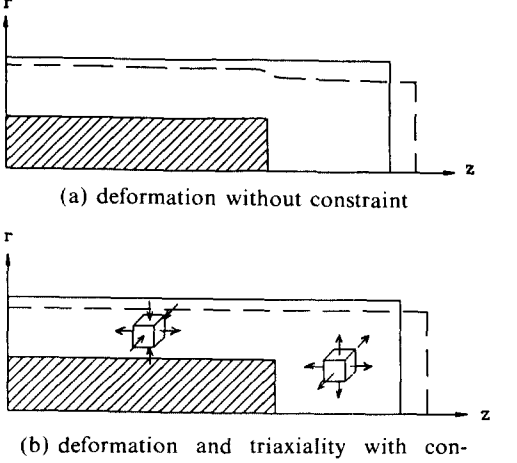

(a) deformation without constraint

(b) deformation and triaxiality with constraint. (In each figure, Dashed line represents deformed shape)

Fig. 4 A schematic of deformed shape with and without constraint and additional stress components produced by constraint effects.

can also be decomposed to the surrounding matrix region Ω_{m1} and the matrix region between fiber ends Ω_{m2} as shown in Fig. 3. This stress grouping is, actually, based on the additionally generated stress components under uniaxial loading due to constraint condition, of which rationale is explained as follows.

Figure. 4(a) and (b) show the schematic of deformed shape with and without constraint case. In the unconstrained model shown in Fig. 4(a), which has a traction free side wall, the fiber end region is more deformed radially and tangentially than that of the side wall constrained case. In domains of Ω_f, Ω_{m1} and Ω_{m2}, presumably, additional stresses are produced due to constraint effects. In domains of Ω_f and Ω_{m1}, compressive radial and hoop stresses are generated, whereas additional tensile radial and hoop stresses in Ω_{m2} are produced as shown in Fig. 4 (b). Note that, the domain boundaries of Ω_{m1} and Ω_{m2} should not exactly be a straight line from the fiber tip but a little shifted presumably. However, grouping of Ω_{m1} and Ω_{m2} provides a general feature of constraint effects. Thus far, stress grouping was intended to analyse domains of Ω_f, Ω_m, Ω_{m1} and Ω_{m2} so as to compare field quantities of the constraint case to those of the unconstraint case.

3.2 Materials and experiments

The experimental monotonic tensile stress-strain curves for Al 2124 and Al 2124 reinforced by 20 vol. % SiC fiber were performed using strain controlled tensile test at the strain rate of 10^{-3}/sec in an Instron 1330 Servo-Hydraulic test machine at room temperature. The unreinforced Al 2124 was processed in identical fashion to the composite, namely, by a powder metallurgy process involving hot processing above the solidus followed by hot extrusion. The SiC fibers are approximately 1μm in diameter with an average aspect ratio of 4 and tend to be aligned in the extrusion direction which corresponds to the longitudinal axis of the tensile samples. After machining, the samples were heat treated for T-6 condition. All tensile tests were performed in accordance with the ASTM standard test method, Tension testing of metallic materials (ASTM E-8).

From the matrix test data, a bilinear representation of the matrix stress-strain curve was used for computer simulation. Thus, the stress-strain characteristics of the matrix are defined by the elastic modulus, yield stress and work hardening rate (tangent modulus). These characteristics were measured at room temperature on the PM 2124 Al alloy and were found to be $E_m=70GPa$, $\sigma_{my}=336MPa$ and $E_T=1.04GPa$, respectively. Other material properties selected are $\nu_m=0.33$ for matrix and $E_f=480GPa$, $\nu_f=0.17$ for reinforcement (Taya and Arsenault, 1989; Kim, 1994b). Here, E is Young's modulus, E_T is tangent modulus, δ_{my} is matrix yield stress and ν is Poisson's ratio.

The fiber and matrix materials were assumed to be isotropic and the elastic constants were assumed to be temperature independent. The experimental data for compressive stress-strain curves was not needed for input data because the isotropic hardening rule was implemented in this study. Further, thermally induced residual stresses were neglected and those computations are to be performed in the subsequent work.

4. Results and Discussion

4.1 Composite behavior

To obtain the stress-strain hysteresis behavior numerically, the applied far field strain $\in_c$ was subsequently loaded from 0% (Origin) to 1% (point A), 1% to 0% (point B), 0% to-1% (point C), -1% to 0% (point D), and 0% to 1% (point E), as described in Fig. 5. To solve nonlinear analysis, 25 small load steps of which step has maximum 20 iterations were used incrementally by $\Delta\varepsilon_c=0.04\%$. The calculated hysteresis loops of five cycles for isotropic matrix are shown in Fig. 6. The result shows that isotropic matrix was nearly saturated to the matrix ultimate tensile strength even in five cycles. This behavior gives a verification of the program and the theory.

Figure 7 shows the composite stress-strain hysteresis loop with and without constraint conditions. The tensile and compressive stress-strain behavior of each curve shows a similar fashion as expected. However, it is shown that both loops

make a functional difference in the flow regime. The unconstrained RVE shows a little composite strengthening effect, which is the unrealistic constitutive behavior as discussed in the monotonic tensile loading case (Kim, 1992 ; Kim 1994a).

4.2 Role of matrix

Figure 8 shows a decomposed matrix stress-strain relation using stress grouping approach. A slight difference between the constrained and unconstrained RVE is shown for the overall matrix strength. It suggests that fiber/fiber interactions affect to the matrix strength in a domain dependent manner. Therefore, it is inferred that the composite strengthening does not stem from the matrix directly though it generates the factor to enhance the strength.

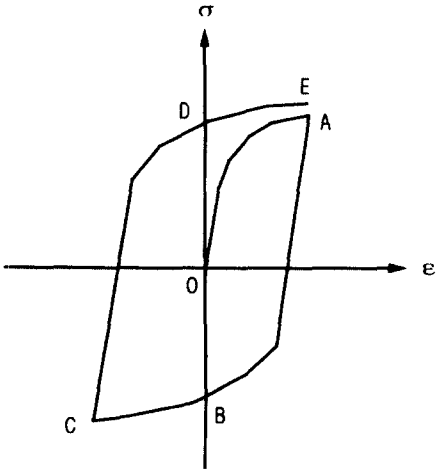

Fig. 5 A schematic of stress-strain hysteresis loop.

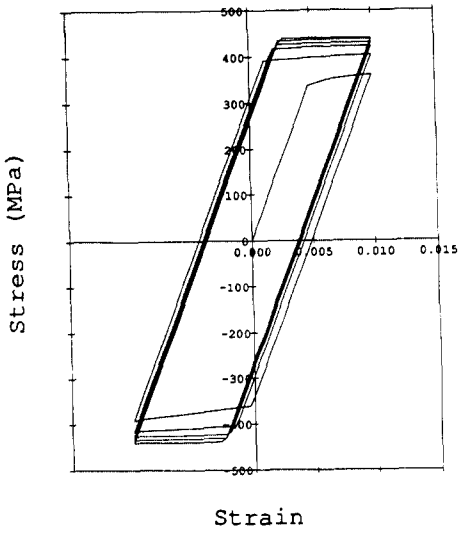

Fig. 6 Calculated hysteresis loops of five cycles for isotropic matrix.

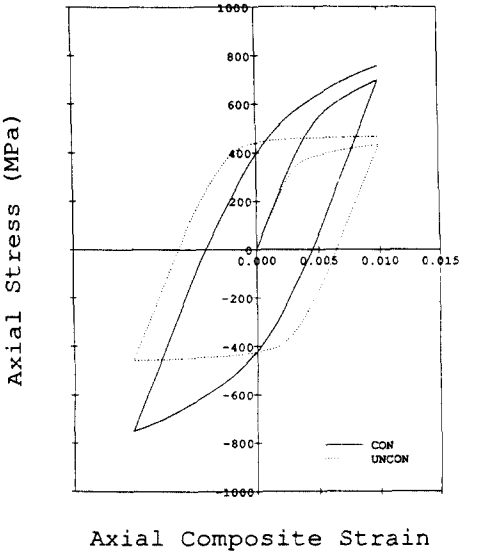

Fig. 7 Numerically predicted stress-strain responses for fully reversed loading between far-field composite strains of 1% and -1% with and without constraint conditions.

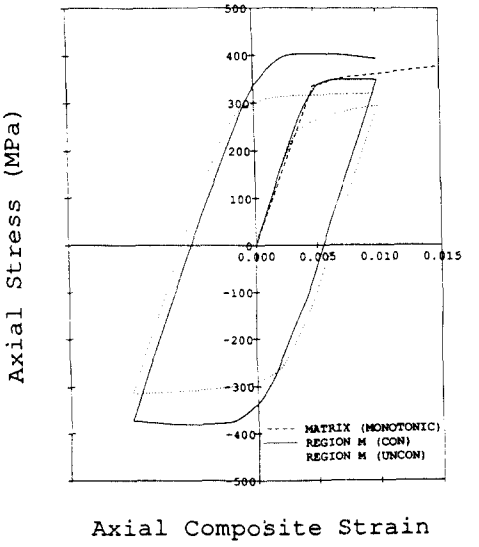

Fig. 8 Total matrix average axial stresses for a hysteresis loop with and without constraint conditions.

Accordingly, matrix region Ω_m has been divided into Ω_{m1} and Ω_{m2} as described in Fig. 3. Hence, some difference of constraint effect is shown in the domain Ω_{m1} (*see* Fig. 9) whereas the pronounced difference is shown in the domain Ω_{m2} (*see* Fig. 10). Therefore, it is inferred that the constraint condition influences in the domain Ω_{m2} substantially compared to the domain Ω_{m2}. Interestingly, the results of domains of Ω_c and Ω_{m2} show the same values as they should (*see* Figs. 6 and 9). In axisymmetry, the sectional equilibrium condition is required in the axial plane. Thus, the results of homogeneous Ω_{m2} domain must follow the composite behavior.

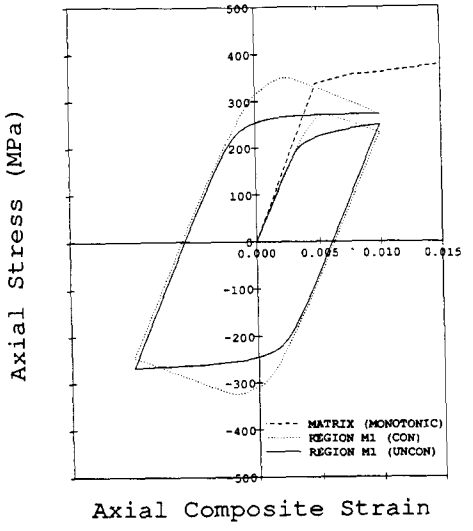

Fig. 9 Decomposed matrix average axial stresses in the region of Ω_{m1} for a hysteresis loop with and without constraint conditions.

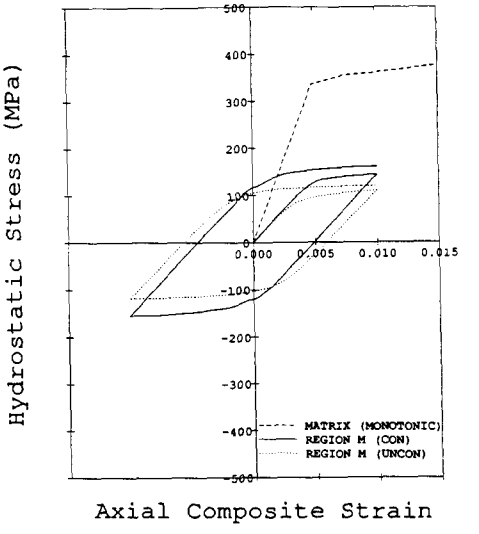

Fig. 11 Totla matrix average hydrostatic stresses for a hysteresis loop with and without constraint conditions.

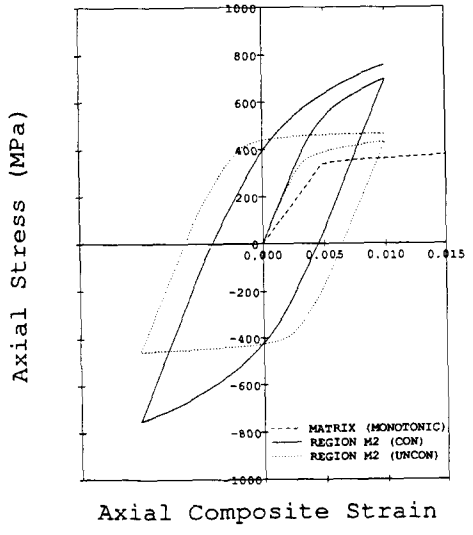

Fig. 10 Decomposed matrix average axial stresses in the region of Ω_{m2} for a hysteresis loop with and without constraint conditions.

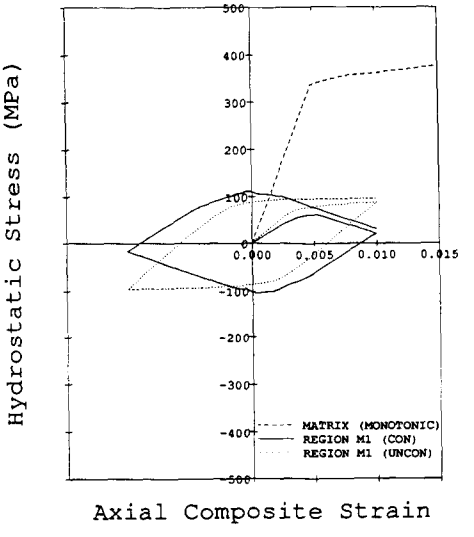

Fig. 12 Decomposed matrix average hydrostatic stresses in the region of Ω_{m1} for a hysteresis loop with and without constraint conditions.

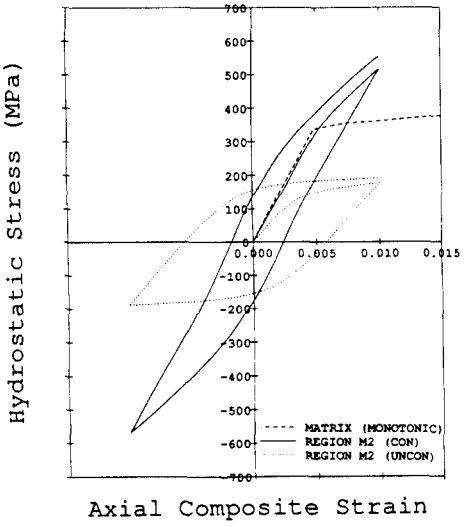

Fig. 13 Decomposed matrix average hydrostatic stresses in the region of Ω_{m2} for a hysteresis loop with and without constraint conditions.

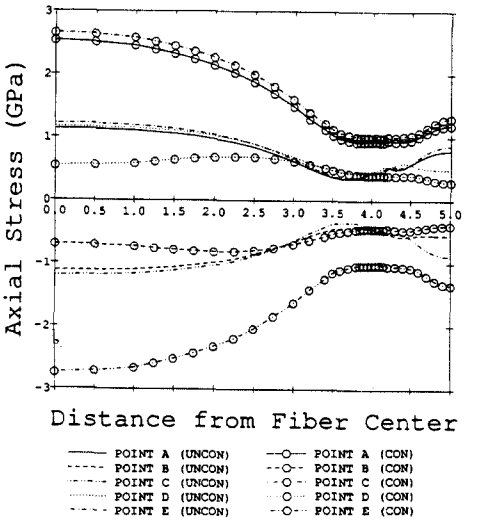

Fig. 14 Fiber stresses on the center line as a function of distance normalized by fiber radius with and without constraint conditions.

Matrix hydrostatic stress-strain hysteresis loops in the domains of Ω_m, Ω_{m1} and Ω_{m2} for the constrained and unconstrained RVEs are shown in Figs. 10 to 13, respectively. In the domains of Ω_m and Ω_{m1}, however, the pronounced constraint effects on hydrostatic stresses are not shown, whereas hydrostatic stresses in domain Ω_{m2} show markedly high values because of the additionally generated tensile triaxiality for the constrained RVE. This enhancement of hydrostatic stresses results in the expansion of yield surface, which prohibits the extensive plastic deformation. On the contrary, hydrostatic stresses in the domain Ω_{m1} for the constrained RVE decrease as the far field load increases due to the additionally generated opposite radial stress component. Thus far, the resulting matrix hydrostatic stress for the constrained RVE shows slightly higher values than that of the unconstrained RVE. It is found that the pronounced constraint effects on hydrostatic stresses stem from the additionally generated tensile triaxiality.

4.3 Role of fiber

Figure 14 describes the fiber stresses at five points (A, B, C, D, and E) on the hysteresis loop. Note that the points located were explained in the previous section. The fiber average axial stresses of the unconstrained RVE indicate that the fiber stresses are quite limited. At the unloaded state (ε_c=0%), such as points B and D, it is shown that the substantial fiber stresses are remaining due to the plasticity in the matrix. Likewise, the constrained RVE also shows some stresses at the unloaded state though the magnitude is not so high. Further, the fiber stresses of constrained RVE are well over 2 GPa at 1% far field composite strain. The implication of this result indicates that the major composite strengthening mechanism stems from fiber strengthening generated by sectional equilibrium in the axial direction based on tensile triaxiality. The high fiber stress intensification is important from the standpoint of potential fiber fracture during the deformation of MMCs. Preliminary results (Murdeshwar, 1989) suggest that the fiber actually fracture during tensile straining of MMCs.

4.4 Comparison with other strengthening theories

The basic objective of strengthening theories is to predict composite response given the properties, geometry and the relative amounts of each phase. Within the context of small strain theory,

exact volume averaging (Cho and Gurland, 1988) gives the average stress and the average strain tensors in the composite as

$$\sigma_{ave} = c_i \sigma_i \tag{23}$$

$$\varepsilon_{ave} = c_i \varepsilon_i \tag{24}$$

where c_i is the volume concentration of phase i, $\sum c_i = 1$, and where σ_i and ε_i are, respectively the average stress tensor and the average strain tensor in phase i. The approximation involved in various theories concerns the estimates used for σ_i and ε_i. Self-consistent methods also provide approximate predictions of composite elastic response that explicitly account for phase geometry. For instance, Eshelby's ellipsoidal inclusion method (Eshelby, 1957) has been successfully applied to predict both the modulus and yield strength of short fiber composites (Taya and Arsenault, 1987). However, this model including the relaxation model (Mori and Tanaka, 1973) is restricted to ellipsoidal reinforcement geometry for which case the internal reinforcement stress is assumed to be uniform. It is well known that for the case of rod-like fiber geometries, uniform reinforcement stresses are obtained only at sufficiently large aspect ratios. The uniform internal reinforcement stress results from the physical nature of the ellipsoidal geometry for which case both normal and shear load transfer to the reinforcement occurs along the entire reinforcement/matrix boundary. For an axially aligned cylindrical geometry, however, with the load applied in the axial direction, the normal stress transfer occurs only at the fiber end and the stress transfer along the fiber length is purely of a shear nature. This shear stress transfer gives rise to the known variation of the fiber axial stresses (Piggot, 1980). This phenomenon is related to the plastic deformation evolution that is important to appreciate the strengthening induced by fiber/fiber interactions.

Various approximate theories of composite strengthening have also been proposed that directly relate the composite yield strength to the yield strength of the matrix besed on enhanced dislocation density in the matrix. However, since the composite stress-strain curve is typically rather smooth, characterization of the stress-strain response in terms of a yield strength is incomplete. Further, it is not observed experimentally for the 2124 SiC whisker composite system where the range of microhardness values for the composite matrix is roughly the same as that of the control alloy (Christman, Needleman, and Suresh, 1989).

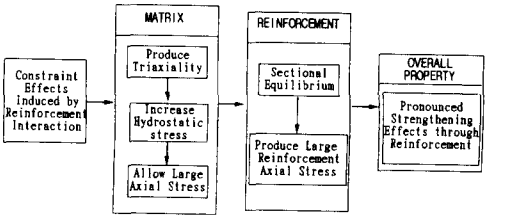

Fig. 15 Block diagram of strengthening mechanism in MMCs.

Finally, the strengthening mechanism arising from constrained plastic flow and triaxiality in the ductile matrix due to the presence of brittle reinforcements was investigated in detail through the constraint-unconstraint comparative study and stress grouping approach. It was found that this approach provides a rationale through the constitutive characteristics in MMCs. Results shown in previous sections seem that the formation of triaxiality due to fiber/fiber interaction is the major contributor for composite strengthening. As a result, a brief strengthening mechanism integrating each strengthening component is delineated in Fig. 15, which suggests that the major strengthening stem from the sectional equilibrium in axial direction and triaxiality in the matrix due to constraint effects.

5. Conclusions

The constitutive characteristics of MMCs were studied numerically with the objective of investigating the tensile and compressive composite behavior and the major strengthening contributor. By means of the stress grouping approach, a constraint-unconstraint comparative study based on stress-strain hysteresis loop was performed and several sequences with key elements of strengthening were identified. It was found that the con-

strained plastic flow and triaxiality in the matrix gives a substantial contribution of composite strengthening both for the tensile and compressive loading.

References

Agarwal, B. D., Lifsitz, J. M. and Broutman, L. J., 1974, "Elastic-Plastic Finite Element Analysis of Short Fiber Composites," *Fiber Science and Technology,* Vol. 7, pp. 45~62.

Aresenault, R. J., 1983, "Interfaces in Metal Matrix Composites," *Scripta Metallurgica,* Vol. 18, pp. 1131~1134.

Arsenault, R. J., 1984, "The Strengthening of Aluminum Alloy 6061 by Fiber and Platelet Silicon Carbide," *Materials Science and Engineering,* Vol. 64, pp. 171~181.

Arsenault, R. J. and Fisher, R. M., 1983,"Microstructure of Fiber and Particulate SiC in 6061 Al Composites," *Scripta Metallurgica,* Vol. 17, pp. 67~71.

Arsenault, R. J. and Pande, C. S., 1984, "Interfaces in Metal Matrix Composites," *Scripta Metallurgica,* Vol. 18, pp. 1131~1134.

Arsenault, R. J. and Shi, N., 1986, "Dislocation Generation Due to Differences between the Coefficients of Thermal Expansion," *Materials Science and Engineering,* Vol. 81, pp. 175~187.

Arsenault, R. J. and Taya, M., 1987, "Thermal Residual Stress in Metal Matrix Composite," *Acta Metallurgica,* Vol. 35, pp. 650~659.

Cho, K. and Gurland, J., 1988, *Metallurgical Transactions,* Vol. 19A, p. 2027.

Christman, T., Needleman, A. and Suresh, S., 1989, "An Experimental and Numerical Study of Deformation in Metal-Ceramic Composites," *Acta Metallurgica,* Vol. 37, No. 11, pp. 3029~3050.

Cook, R. D., Malkua, D. S. and Plesha, M. E., 1989, "*Concepts and Applications of Finite Element Analysis*," John Wiley and Sons, Third Edition, pp. 163~295.

Derby, B. and Walker, J. R., 1988, "The Role of Enhanced Dislocation Density in Strengthening Metal Matrix Composites," *Scripta Metallurgica,* Vol. 22, pp. 529~532.

Divecha, A. P., Fishman, S. G. and Karmarkar, S. D., 1981, "Silicon Carbide Reinforced Aluminum - A Formable Composite," *Journal of Metals*, Vol. 33, No. 9, pp. 12~17.

Drucker, D. C., 1965, *High Strength Materials,* John Wiley & Sons, Inc., First Edition, Edited by Zackay, V. F., Chapter 21, Engineering and Continuum Aspects of High-Strength Materials, pp. 795~833.

Eshelby, J. D., 1957, "The Determination of the Elastic Field of an Ellipsoidal Inclusion, and Related Problems," *Proceedings of the Royal Society,* London, Vol. A241, pp. 376~396.

Kelly, A. and MacMillan, N. H., 1986, *Strong Solid,* 3rd Edition, Clarendon Press, Oxford, p. 240.

Kim, H. G., 1992, "Micromechanics of Deformation in Short Fiber or Whisker Reinforced Metal Matrix Composites," Ph. D Dissertation, Department of Mechanical Engineering, University of Massachusetts, Amherst, MA, USA.

Kim, H. G., 1994a, "Assessment of Plastic Constraint Effects Induced by Whisker Interactions in Whisker Reinforced Metal Matrix Composites," *Journal of the Korean Society for Composite Materials*, Vol. 7, No. 3, pp. 1~10.

Kim, H. G., 1994b, "Stress Transfer in Shear Deformable Discontinuous Composites," *KSME Journal*, Vol. 8, No. 4, pp. 475~484.

Kim, H. G., Chang, S. H., Chang, D. S. and Chung, S. K., 1994, "A Numerical Study Using Micromechanics Model for Metal Matrix Composites," *Proceedings of Materials Research Society of Korea*, pp. 133~136.

Koss, D. A. and Copley, S. M., 1971, "Thermally Induced Residual Stresses in Eutectic Composites," *Metallurgical Transactions*, Vol. 2, pp. 1557~1560.

Levy, A. and Papazian, J. M., 1991, "Elastoplastic Finite Element Analysis of Short Fiber Reinforced SiC/Al Composites : Effects of Thermal Treatments," *Acta Metallurgica,* Vol. 39, No. 10, pp. 2255~2266.

Mori, T. and Tanaka, K., 1973, "Average Stress in Matrix and Average Elastic Energy of Materials with Misfitting Incl usions," *Acta Metallurgica,* Vol. 21, pp. 571~574.

Murdeshwar, N., 1989, "Fracture Development in a 20 Volume Percent Silicon Carbide Whisker Reinforced Al 2124 Metal Matrix Composite," M. S. Thesis, University of Massachusetts at Amherst, MA, USA.

Nair, S. V. and Kim, H. G., 1991, "Thermal Residual Stress Effects on Constitutive Response of a Short Fiber or Whisker Reinforced Metal Matrix Composite," *Scripta Metallurgica,* Vol. 25, No. 10, pp. 2359~2364.

Nair, S. V., Tien, J. K. and Bates, R. C., 1985, "SiC Reinforced Aluminum Metal Matrix Composites," *International Metals Review,* Vol. 30, No. 6, pp. 275~290.

Nardone, V. C., 1987, "Assessment of Models Used to Predict the Strength of Discontinuous Silicon Carbide Reinforced Aluminum Alloys," *Scripta Metallurgica*, Vol. 21, pp. 1313~1318.

Nardone, V. C. and Prewo, K. M., 1986, "On the Strength of Discontinuous Silicon Carbide Reinforced Aluminum Composites," *Scripta Metallurgica,* Vol. 20, pp. 43~48.

Piggot, M. R., 1980. "Load Bearing Fiber Composites," *Pergamon Press,* pp. 83~99.

Takao, Y., Chou, T. and Taya, M., 1982, "Effective Longitudinal Young's Modulus of Misoriented Short Fiber Composites," *Journal of Applied Mechanics,* Vol. 49, pp. 536~540.

Taya, M., and Arsenault, R. J., 1987, "A Comparison between a Shear Lag Type Model and an Eshelby Type Model in Predicting the Mechanical Properties of Short Fiber Composite," *Scripta Metallurgica,* Vol. 21, pp. 349~354.

Taya, M. and Arsenault, R. J., 1989, "Metal Matrix Composites, Thermomechanical Behavior," Pergamon Press, NY. Taya, M. and Mori, T., 1987, "Dislocations Punched-Out around a Short Fiber Metal Matrix Composite Subjected to Uniform Temperature Change," *Acta Metallurgica,* Vol. 35, No. 1, pp. 155~162.

Vogelsang, M., Arsenault, R. J. and Fisher, R. M., 1986, "An In-Situ HVEM Study of Dislocation Generation at Al/SiC Interfaces in Metal Matrix Composites," *Metallurgical Transactions* A, Vol. 17A, pp. 379~388.